JOURNAL OF AIRCRAFT
Vol. 30, No. 5, Sept.–Oct. 1993

Aerodynamic Calculation of Complex Three-Dimensional Configurations

F. Roggero* and R. Larguier†
Office National d'Etudes et de Recherches Aérospatiales, Châtillon, France

A three-dimensional code called ECOPAN, based on an "inner Dirichlet" boundary condition, has been developed at ONERA. It is currently used to calculate a wide variety of complex aerodynamic configurations. Thus, the future European Ariane 5 launch vehicle has been evaluated in the takeoff phase. It is shown that the change from the automatic version to the Hermes version results in a decrease of the launcher total stability. This decrease is moderated by a favorable interaction of Hermes wake on the lower part of the launcher. A complete Airbus aircraft has been calculated in its takeoff configuration with flaps and slats extended and with a simulation of engine primary and secondary fluxes. The increase in lift due to a plane of symmetry simulating the ground effect has been estimated to be of the order of a few percents, which is in agreement with flight test results. In these two applications the ECOPAN code has demonstrated its versatility, its operational status, and its aptitude to perform parametric analyses in subsonic flow.

Nomenclature

$[A]$ = influence coefficient square matrix
C_L = lift coefficient
C_M = pitching moment coefficient
C_N = normal force coefficient
C_p = pressure coefficient
dS = surface element
dV = volume element
L_{ref} = diameter of Ariane 5 central body, m
M = Mach number
$\boldsymbol{n}$ = normal unit vector
S = surface
$\boldsymbol{V}$ = velocity vector
$\boldsymbol{v}$ = perturbation velocity vector
$[W]$ = column vector describing the boundary conditions
X = longitudinal position, m
X_f = position of the aerodynamic center of the interaction effect, m
X_m = position of the center of gravity, m
α = incidence angle
β = sideslip angle
η = wingspan section
μ = doublet strength
σ = source strength
Φ = velocity potential
φ = perturbation velocity potential

Subscripts
b = body
e = outer (V_e or Φ_e) or exhaust (S_e)
en = external normal value
i = inner
P = point relative to the observer
Q = integration variable
α = incidence gradient
η = spanwise local value
∞ = freestream conditions

Presented as Paper 90-6.4.3 at the 17th Congress of the International Council of the Aeronautical Sciences, Stockholm, Sweden, Sept. 9–14, 1990; received Jan. 1, 1992; revision received May 7, 1992; accepted for publication May 7, 1992.

*Research Engineer, Applied Aerodynamics Division, Aerodynamics Department.
†Head, Applied Aerodynamics Division, Aerodynamics Department.

Introduction

THE three-dimensional ECOPAN code was developed at ONERA to meet a wide variety of demands, including those of the Ariane and Airbus European programs. For these types of configurations, the panel method approach is still the most efficient tool as it uses only a surface grid which is relatively easy to generate. In addition, recent developments of the method also make it possible to aerodynamically evaluate such complex configurations in reasonable computing time.

In this article, the ECOPAN method is briefly presented first. This three-dimensional steady inviscid flow calculation code is based on research by Rehbach at ONERA on "inner Dirichlet" code, and has been perfected by Kirrmann[1] and Roggero. In this method, the boundary condition used concerns the inner potential whose value is chosen so that the potential remains regular outside the bodies, thereby making the method less sensitive to the mesh irregularity than the codes using Neumann-type boundary conditions. Therefore, the inner Dirichlet condition provides a very good mass flow conservation for guided flows, minimizes leakage through the surfaces in strong interaction zones, and removes the defects in the calculation of surfaces with concave areas, such as wings with supercritical profiles. This type of method appeared around 1979 in the U.S. and, is now widely used.[2,3] Most new panel codes, like VSAERO,[4–8] QUADPAN,[9] S-SUB2,[10] HISSS,[11,12] etc., are based on this new formulation, or at least they contain it as an option or as a particular case of a more general solution, as in PAN-AIR.[13,14]

A validation study is then presented by comparing ECOPAN results with those of an ONERA finite-element code, for the DLR F4 civilian aircraft wing and an open engine nacelle. Some comparisons are also made with wind-tunnel tests on the Hermes European shuttle. To illustrate the code capabilities, two typical applications are presented for complex configurations. The future European Ariane 5 launch vehicle has been evaluated in its subsonic flight phase with and without the Hermes shuttle. A complete Airbus-type aircraft geometry has been calculated with flaps and slats extended in takeoff configuration.

ECOPAN Code Presentation

The ECOPAN code is used to compute subsonic inviscid flows around three-dimensional bodies such as launchers or complete aircraft.

It is an integral-type method, based on the solution of the Laplace equation applied to the velocity potential

$$\Delta\Phi = 0 \quad \text{with} \quad V = \nabla\Phi \tag{1}$$

The part of the flow potential that is due to the body is modeled by surface distributions of combined doublet-source panels that are elementary solutions of the Laplace equation.

Basic Integral Equation for the Thick Body Case

The application of the third Green equation (Green-Ostrogradski theorem or divergence formula

$$\int\int\int \nabla\cdot f \, dV = \int\int n\cdot f \, dS$$

applied to the vector field $f = \Phi\nabla(1/r) - \nabla\Phi/r)$ gives an integral equation between the potential at a point P and the source and doublet strength over S

$$\Phi_P = \left(\frac{1}{4\pi}\right)\int\int_S \mu n\cdot\nabla_Q\left(\frac{1}{r}\right) dS_Q - \left(\frac{1}{4\pi}\right)\int\int_S \left(\frac{\sigma}{r}\right) dS_Q + \Phi_{\infty P} \tag{2}$$

with

$$\mu = \Phi_e - \Phi_i \tag{3}$$

$$\sigma = n\cdot(\nabla\Phi_e - \nabla\Phi_i) \tag{4}$$

$$r = |X_Q - X_P|$$

The source and doublet strengths σ and μ being unknown, the solution requires two boundary conditions.

Boundary Conditions

The ECOPAN code uses an inner Dirichlet condition, which consists of imposing the potential of the virtual inside flow in addition to the condition on the external normal velocity. This way the sources take explicit values that depend on external normal velocities, and the doublets are the solution of an integral equation prescribing the condition on the inner potential.

An inner potential is usually set corresponding to free-stream boundary conditions, i.e.

$$\Phi_i = \Phi_\infty \tag{5}$$

Source Strengths

Equation (4) says that the source strengths are equal to the difference between external and internal normal velocities:

$$\sigma = V_e\cdot n - V_i\cdot n \tag{6}$$

In the case of a surface with no mass through flow, the boundary conditions $\Phi_i = \Phi_\infty$ and $V_e\cdot n = 0$ determine the source strength:

$$\sigma = -V_\infty\cdot n \tag{7}$$

It is possible to impose a nontangential velocity on the body surface by means of a normal velocity condition of the form

$$V_e\cdot n = V_{en}$$

V_{en} is set equal to zero when the slip condition is desired, and not zero in the case of a surface with a mass flow condition, e.g., to simulate a boundary layer by a transpiration model, or a mass flow through an engine nacelle.

Doublet Strengths

The doublet strengths are obtained writing the boundary conditions [Eq. (5)] inside the body:

$$\underbrace{\frac{1}{4\pi}\int\int_S \mu n\cdot\nabla_Q\left(\frac{1}{r}\right) dS}_{\text{potential induced by the doublets of unknown strengths } \mu} = \underbrace{\frac{1}{4\pi}\int\int_S \frac{\sigma}{r} dS}_{\text{known term}} \qquad \forall P \in S$$

Using a discretized form, this equation can be written in the following linear system:

$$[A][\mu] = [W]$$

where $[A]$ depends only on the body geometry, and $[\mu]$ is the unknown doublet strength column vector. The second member $[W]$ is known. This resulting linear system, in which the unknowns are the doublet strengths, is solved by a lower upper bloc method with asynchronous input/output. As the rank of such systems with full matrices can exceed 10,000, complete overlapping between computation and input/output considerably reduces the cost.

Velocity Calculation

The inner Dirichlet condition involves a very fast calculation of the surface velocities. Indeed, only the normal and tangential velocity jumps, due to the source and doublet distributions, are added to the imposed internal velocity, i.e.

$$V_e = V_i + \sigma n + (\nabla\mu)_S$$

$$V_e = V_\infty + \sigma n + (\nabla\mu)_S$$

$(\nabla\mu)_S$ being the surface gradient of the doublet strength.

Wakes

The wing vortex sheets are discretized by wake doublet panels, equivalent to a vortex lattice extending infinitely downstream. The vortex circulation is calculated by applying an emission condition (equivalent to a Kutta-Joukowski condition) at the trailing edge of every profile. Some options are available to express this last condition according to whether or not the trailing edge is thick and whether or not the emission condition is linearized.

Code Extensions

A Prandtl-Glauert compressibility correction can be used to compute slightly compressible flows. For complex configurations, a free-wake geometry calculation option can be used, but this is a costly iterative calculation.

Particular Case of Thin Surfaces

When the thickness of the obstacle can be neglected, a Neumann condition is used to solve the singularity strength by a normal velocity condition on constant-strength doublet-type panels. The doublet strengths are obtained solving the boundary condition on the surface

$$v\cdot n = V_{en} - n\cdot V_\infty$$

in the form

$$\underbrace{\int\int_{S_b + S_e} v_\mu\cdot n \, dS}_{\text{velocity induced by doublets of unknown strengths } \mu} = \underbrace{V_{en} - n\cdot V_\infty - \int\int_{S_b} v_\sigma\cdot n \, dS}_{\text{known term}}$$

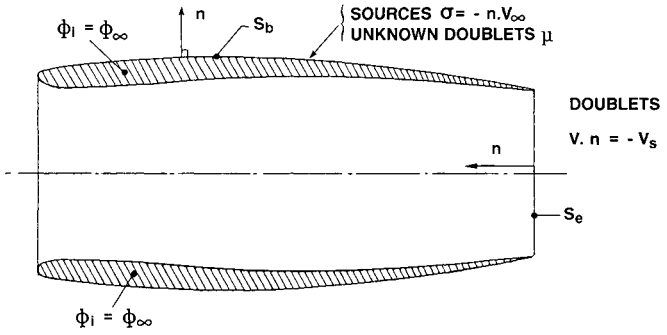

Fig. 1 Schematic representation of an engine nacelle calculation with mass-flow control.

Instead of stipulating a Kutta-Joukowski-type condition, this formulation is used to regulate the exit velocity in the exhaust plane of an engine nacelle directly, by adding a doublet surface in this plane that is regulated by a Neumann condition setting the value of the normal velocity at collocation points (Fig. 1).

ECOPAN Code Evaluation

Comparison with Finite-Element Code

Calculation of the DLR F4 Wing

The DLR F4 research wing of transport aircraft-type was calculated by ECOPAN using the grid presented in Fig. 2. The result was compared to a computation by finite-element method[15] at two Mach numbers, $M = 0$ and $M = 0.3$. Figures 3 and 4 show the local pressure distribution at the wingspan section $\eta = 0.325$, and the spanwise distribution of the normal force $C_{N\eta}(\eta)$ at $M = 0$. Figure 5 presents the relative discrepancies in normal force coefficient between $M = 0$ and $M = 0.3$, as a percent. It is worth noting that the compressible flow effects are quite similar for the two codes ($\Delta C_{N\eta}/C_{N\eta}$ between 3 and 4%).

Calculation of an Open Engine Nacelle

The flow through an open engine nacelle (geometry shown in Fig. 1) was also calculated to validate the method for guided flow.[1] Figure 6 shows the comparisons between the pressure coefficient distribution obtained from the two-dimensional axisymmetric finite-element method with an exit mean velocity $V_S = 0.865$, and the same distribution obtained from the ECOPAN method with a velocity of $V_S = 0.90$ at the exhaust plane. The comparison between the pressures obtained by the two methods is good; only the leading-edge peaks (inside and outside) present any noticeable discrepancy. This may be a result of the differences in grid precision (exactly axisymmetric mesh of 128 grids per profile for the finite-element method, but 12 sections of 66 cosine-type panels for the ECOPAN method).

Comparison with Experimental Results: Computation and Test of the Hermes Shuttle

The Hermes configuration was computed within the incidence margin $0 < \alpha < 20$ deg at $M = 0.2$. As an example, Fig. 7 shows the result of an ECOPAN computation at $\alpha = 10$ deg and $\beta = 10$ deg. The distribution of the pressure coefficient C_p calculated over the aircraft surface shows that the greatest overvelocities are located near the leading edge on the upper side of the wing profiles farthest outboard, particularly over the winglets, while the regions in compression are located obviously at the nose of the aircraft and over the canopy.

Figure 8 compares the results of the ECOPAN computations with test results. The lift coefficient $C_L(\alpha)$ estimate is very good, the calculated curve falls very close to the experimental curve between 0–20 deg of angle of attack. The moment coefficient C_{M60} estimation is less good, particularly the

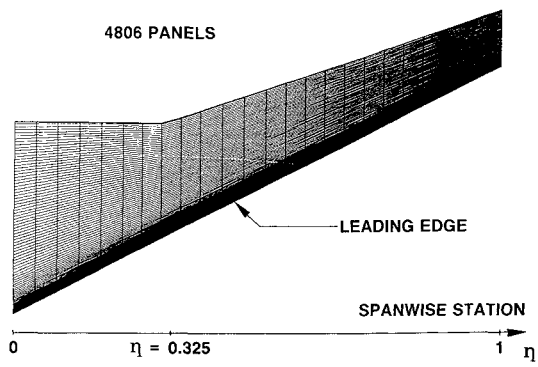

Fig. 2 DLR F4 wing geometry and mesh.

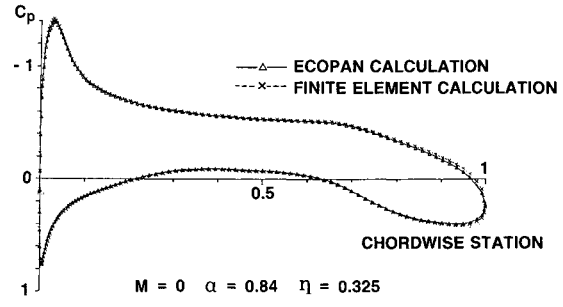

Fig. 3 DLR F4 wing chordwise pressure distribution.

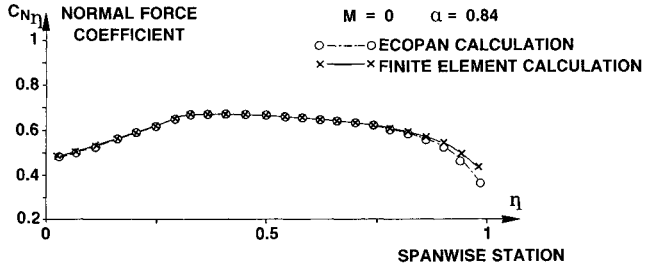

Fig. 4 DLR F4 wing spanwise normal force distribution.

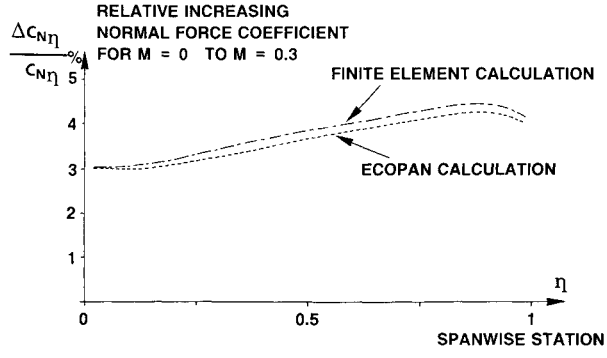

Fig. 5 DLR F4 wing spanwise compressibility effect.

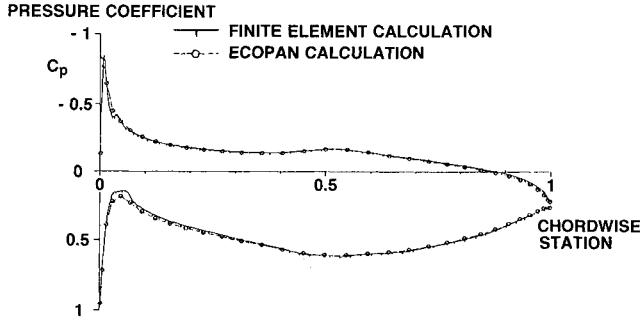

Fig. 6 Pressure distribution on an axisymmetric open-engine nacelle.

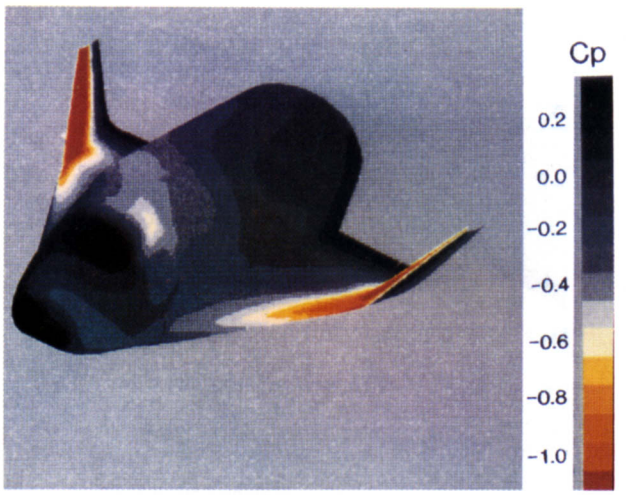

Fig. 7 ECOPAN pressure field computation on the Hermes shuttle (M = 0.2; α = 10 deg; β = 10 deg).

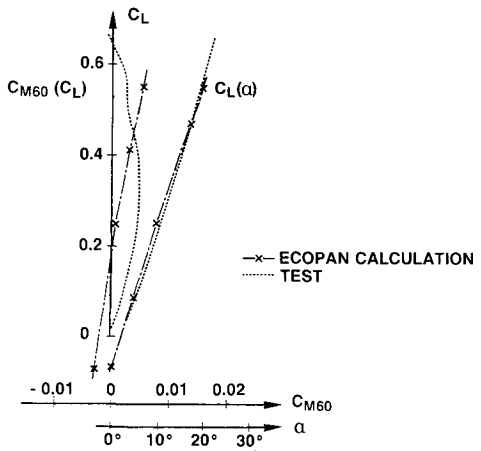

Fig. 8 Hermes shuttle: comparison of normal force and moment calculation with wind-tunnel data.

return to the stability observed in the test at incidences above α = 10 deg, which is not predicted by the ECOPAN computation. However, the discrepancies observed between the computation and the test are quite acceptable considering the hypothesis of the computation (inviscid flow, base flow condition, no wake vortex deformation at high angles of attack, and no consideration of leading-edge vortex flows).

Ariane 5 Launcher Applications

A complete Ariane 5 launcher in takeoff phase was calculated to determine how different architectural configurations of the automatic and Hermes versions would behave.

First, the surface grid is generated from the geometric definition of the launcher. It is worth noting that the specific grid generator programs were developed as ECOPAN improvements for the needs of the Ariane 5 study case. The last part of the study is an analysis of the longitudinal aerodynamic characteristics of the launcher at M = 0.5. This study is particularly based on the comparison between computations obtained by ECOPAN and test results. The automatic and Hermes versions are compared to evaluate the Hermes effect over the lower part of the launcher.

Surface Grid Generation

In the case of the Hermes-Ariane 5 configuration, the space plane grid was generated by available CAD software. The rest of the grid (the launch vehicle) was generated by a program developed at ONERA within the framework of the present application, to mesh simple shapes such as spheres, cones, cylinders, etc., or perform geometric transformations

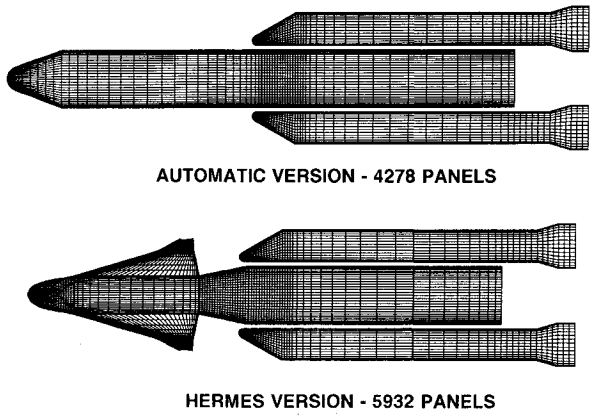

Fig. 9 Ariane 5 launch vehicle grids for the automatic and Hermes configurations.

such as rotations, translations, or similarity transformations. The grid of the automatic and Hermes configurations are divided into 10 and 14 subdomains, respectively. The modularity and interchangeability of some parts of the grid make it easier to define different versions of the Ariane 5 launcher. The division into subdomains also allows partial integrations of the aerodynamic coefficients, at the exit from the ECOPAN processing.

The configuration grids consist of 4278 panels for the automatic version and 5932 for the Hermes version representing half the plane. These are shown in Fig. 9. Note, however, that some parts of the grids, such as the booster nose cones and the Hermes adapter, were refined because the wake effects of the Hermes wings are strong in these areas. The panels facing each other on the boosters and central body are of the same dimensions, to avoid numerical problems due to the small distance between boosters and central body.

Wake for the Hermes Configuration

Geometric Definition

The trailing edge of the Hermes wing is extended by a thin surface modeling the wake. The wake geometry, highly distorted by the presence of boosters downstream of the Hermes trailing edge, is taken as unknown. The method used to approach this geometry consists first of a computation of the Ariane 5-Hermes composite at zero incidence without the wake (nonlifting computation). Streamlines from the Hermes trailing edges are computed by means of a module specially adapted to the ECOPAN code. Finally, the wake is defined in a geometric way. The calculated streamlines cannot always be directly used in defining a wake, because it must be made sure that they do not interact directly with the mesh of the boosters. In this particular case, some local corrections may be necessary. An interactive geometric processing code has been written to make these types of local modifications easier. The local modifications are hardly independent of the user. Indeed, the significant criterium is to avoid the overvelocities created by the wake at the center of the booster meshes. For that the distance between the wake and the grid has to be roughly equal to half a mesh. These modifications concern only the part of the wake along the cylindrical part of the booster and not those around the booster cone where the interaction effects are strong.

Figure 10 illustrates a wake defined this way. The wake grid is drawn tighter around sharp bends and areas of complex geometry (around the cones of the boosters or downstream of the exhaust nozzle) and are extended into the downstream flow by means of panels with high-aspect ratio.

Condition Applied to the Trailing Edge of the Hermes Wing

The trailing edge of the Hermes wing is extended by a thin wake made up of doublet panels. Considering the relatively

thick wing base, special conditions were needed to express the Kutta-Joukowski condition (see the scheme in Fig. 11).

The wake starts from the middle of the base, its shape being given by a preliminary computation of streamlines. The base is closed by two doublet panels whose strengths are determined by those of adjacent trailing-edge panels (μ_1 and μ_2, see Fig. 11). The doublet strength over the wake is found by iterating until the pressures on the upper and lower sides of the trailing edge are equal. During this iteration the wake geometry is not modified.

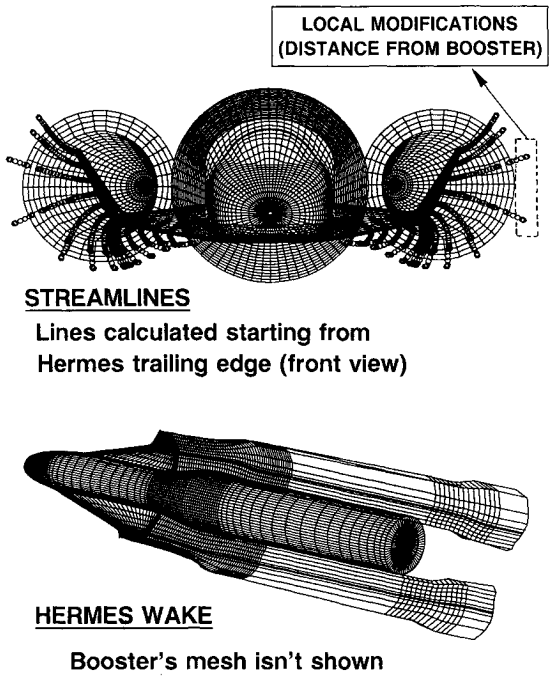

Fig. 10 Hermes wake-sheet geometry.

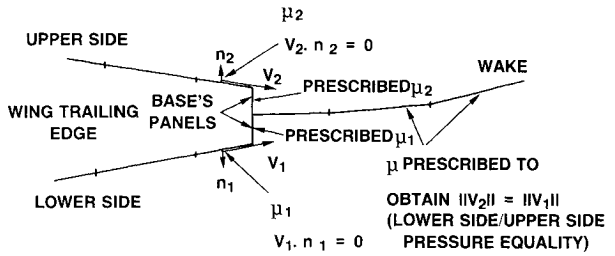

Fig. 11 Boundary conditions around the Hermes wing trailing edge.

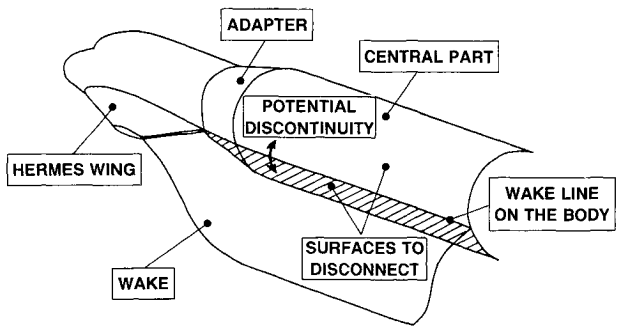

Fig. 12 Schematic representation of the junction between the Hermes wake and the central body.

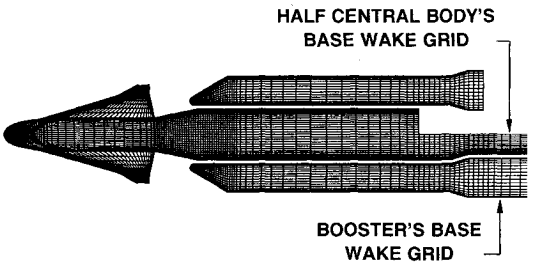

Fig. 13 Booster and central body base: geometric definition of wake lattices.

Special Precaution

The first wake lattice which corresponds to the wing root has to go along a grid line over the adapter and the central body. To have a correct velocity calculation along this line, the surfaces defined by this grid line have to be disconnected, as shown Fig. 12. Indeed, the velocities are determined by the gradient of the doublet distribution, and the gradient calculation must not be modified by the potential jump due to the wake presence.

Base Lattices

Geometric Definition

Wake lattices are also used to model the base areas of the boosters and central body (see Fig. 13). Downstream of the boosters, the lattices extend the base by a cylinder. The lattice from the central body base contracts to avoid the booster exhaust nozzles.

Conditions Applied on the Base Wakes

To reduce the interaction effects observed during the preliminary study, a base flow condition was developed using wakes without any slip condition. This type of wake is better than the extension of the grid by solid surfaces of the cylindrical model-support sting type. However, the slip condition ($\boldsymbol{V}\cdot\boldsymbol{n} = 0$) which is usually used to model the separated area downstream of a base, yields correct results for simple configurations like isolated boosters.

On the other hand, in the case of the Ariane 5 launcher, the central body base is located upstream of the booster exhaust nozzles, so the grid geometry in the continuation of the central body can thereby strongly modify the aerodynamics of the lower parts as the boosters. This problem was solved as follows. The base wakes are made up of doublet panels alone. A constant gradient is imposed in the longitudinal direction (upstream to downstream). Therefore, the unknowns are the value of the gradient and the doublet strengths over every panel at the foot of the wake. The details of the solution of this problem based on the velocity minimization at the base are given in Ref. 16.

Computation Results

All the versions were computed at $M = 0.5$, at two angles of incidence: 1) $\alpha = 0$ deg and 2) $\alpha = 3$ deg. The Mach number was limited to 0.5 because the Prandtl-Glauert compressibility correction used by ECOPAN cannot take the transonic effects into account.

The Hermes configuration was computed with a "prescribed wake," i.e., there is not any iteration on the wake geometry. The same wake geometry is used for the two incidences. This wake geometry is suited for angles of incidence around zero. Note that it will be possible to consider computing a free-wake geometry (iteratively) at the cost of some additional computation time and a tighter drawing in the spanwise direction for the mesh fineness of the Hermes wing. ECOPAN computation results for $M = 0.5$ have been used to characterize the effects changing the upper "payload" part has on the launcher performance by comparing automatic and Hermes versions.

Pressure Distributions

The plot of the pressure distributions computed over the two versions (Fig. 14) shows a major change when the upper part changes, located mainly in the vicinity of booster cones. For the Hermes version, the slope jump of the adapter—

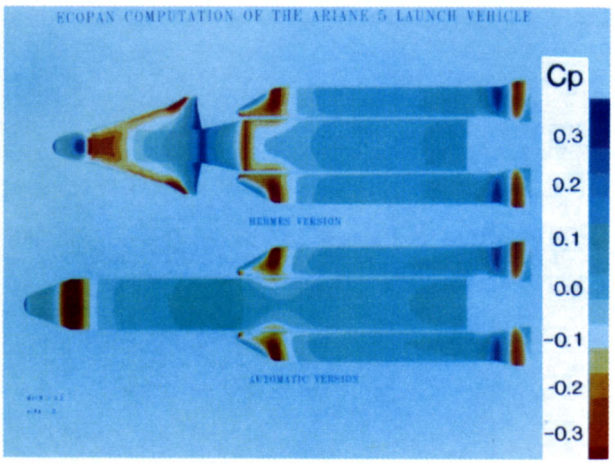

Fig. 14 Ariane 5 launch vehicle: ECOPAN computation of the pressure field.

central body junction is expressed by overvelocities in this area by comparison with the automatic version. The effect of the space shuttle wake is of great importance along the boosters (discrepancies given by the constant-C_p field in Fig. 14) even if this effect seems to be insignificant over the cylindrical parts.

Longitudinal Coefficient

The longitudinal aerodynamic coefficients of the two versions are shown in Figs. 15a and 15b. The normal force coefficients [$C_N(\alpha)$, Fig. 15a] and moment coefficients about the c.g. [$C_M(\alpha)$, Fig. 15b] are solved over the upper part (Hermes and adapter or fairing, depending on the version) and the lower part (central body and boosters).

The change from the automatic version to the Hermes version is expressed in terms of normal force coefficient level by an increase in the global normal force coefficient gradient of $\Delta C_{N\alpha} = 0.069$ (that is, 54.8% of the global $C_{N\alpha}$ for the automatic version). If the weighed force of the upper part is considered, it is noted that the difference in the slopes is higher than this ($\Delta C_{N\alpha} = 0.094$, i.e., 74.4% of the global $C_{N\alpha}$). The increase of normal force coefficient of the upper part is therefore partly compensated by an inverse effect on the lower part.

In terms of moment coefficients about the center of gravity (c.g.) (Fig. 15b), the decreasing of stability due to the presence of Hermes is expressed by a high increase in the gradient of the global moment coefficient, $\Delta C_{M\alpha} = 0.322$ (i.e., 96.8% of the global $C_{M\alpha}$ for the automatic version). As in the previous case, the difference in the $C_{M\alpha}$ for the upper part is higher than the global difference ($\Delta C_{M\alpha} = 0.344$ or 103% of the global $C_{M\alpha}$), the difference corresponding to the lower part with less compensation than for the normal force coefficients. The change from the automatic version to the Hermes version therefore results in a decrease of the launcher total stability, due to the higher normal force coefficient of the upper part of the Hermes version. This decrease is moderated by a favorable interaction of Hermes wake on the lower part of the launcher which must now be necessary to qualify more precisely.

Effect of Hermes over the Lower Part of the Launcher

The disturbance of the aerodynamic field on the lower part of the launcher was studied on the normal force coefficient distributions (for $\alpha = 3$ deg) on the boosters and central body of both the automatic and the Hermes versions. On the boosters (Fig. 16a) a large decrease in lift is noted on the sloping cones (20 m $< X <$ 25 m) due to the presence of Hermes. The effect can be neglected on the cylindrical part but becomes noticeable again at the level of the booster exhaust nozzles (48 m $< X <$ 50 m). On the lower part of the central body (Fig. 16b) the lift decreasing is concentrated under the adapter-central body junction (21 m $< X <$ 23 m); no effects are visible further downstream.

A calculation of the Hermes version at $\alpha = 3$ deg without wake (not presented in this article) showed the importance of the downsteam aerodynamic disturbance due to the Hermes wake and to the adapter. In the case of the central body, the unlifting effect is induced by the adapter and not by the wake. The Hermes version calculations with and without wake show the same effect. In the case of the boosters, the interaction effect is induced by the wake vortex sheet starting from the Hermes wing: the differences between the automatic and Hermes versions, on the one hand, and the Hermes versions with and without wake, on the other, are practically the same.

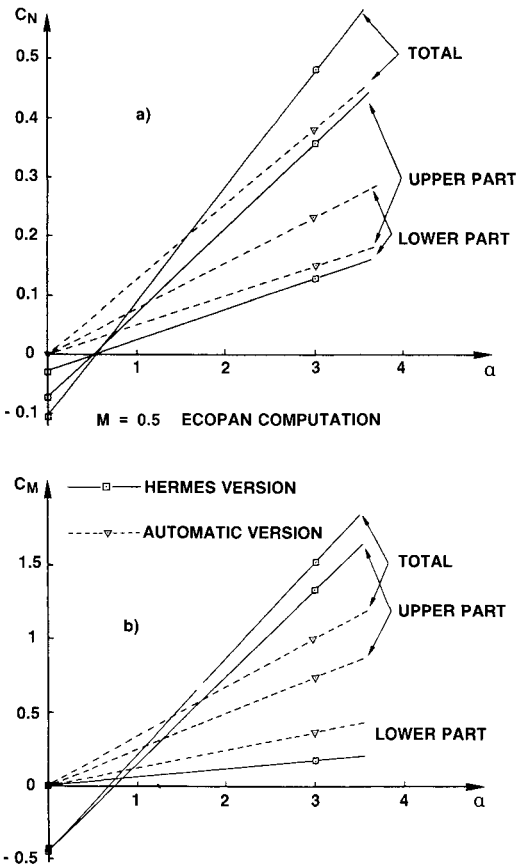

Fig. 15 Ariane 5 launch vehicle: a) normal force coefficient and b) moment coefficient computation.

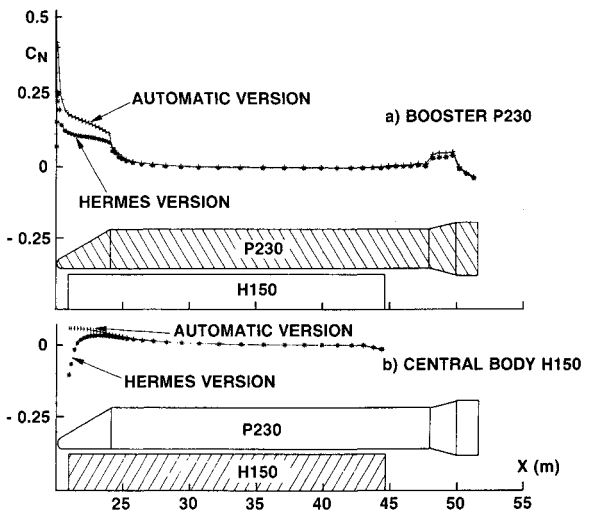

Fig. 16 Longitudinal normal force distribution on lower part of launch vehicle: a) boosters and b) central body.

Table 1 Normal force gradients performed by calculation and test for the two launcher configurations

	Calculation $M = 0.5$		Test $M = 0.8$	
Version	Auto	Hermes	Auto	Hermes
$C_{N\alpha}$TOT	0.1263	0.1955	0.1944	0.2315
$C_{N\alpha}$LP	0.0767	0.0522	0.1423	0.1043
$\Delta C_{N\alpha}$LP	−0.0245 { −0.0240 boost. −0.0005 H150		−0.0380 { −0.0256 boost. −0.0124 H150	
$\frac{\Delta C_{N\alpha}\text{LP}}{C_{N\alpha}\text{TOT}_{\text{Auto}}}$	−19.4%		−19.5%	

Note: $\Delta C_{N\alpha}$ = difference between Hermes and automatic versions.

Comparison with Test Results

Tests conducted at the NLR on the automatic and Hermes versions at Mach 0.8 were also analyzed to characterize the interactions. The test assembly with models equipped with three balances separately weighs the upper part (nose fairing or Hermes and adapter, depending on the version), one isolated booster, and the central part of the launcher (upper part and central body). The normal force gradients (calculated between 0–3 deg of incidence) deduced from test results at $M = 0.8$ and from computations at $M = 0.5$ are presented in Table 1. The weighed force of the lower part (LP) of the launcher (boosters and central body H150 located under the adapter) is deduced from the total (TOT) weighed force for either versions.

A comparison of the interaction effect of Hermes on the lower part of the launcher between these two different Mach numbers has been carried out because there is not any large transonic zone for either case. In the range of incidences investigated ($0 \leq \alpha \leq 3$ deg), the residual transonic effects have no considerable influence on the interaction. Besides at the time of the comparison no test results were available at $M = 0.5$.

The lift decrease on the lower part of the launcher, revealed by the calculation, is also present in the test results ($\Delta C_{N\alpha}$LP, Table 1). The greatest effect is located on the boosters with a good agreement between computation and tests. Over the central body H150, the computed effect is smaller than in the test results. The total difference on the lower part ($\Delta C_{N\alpha}$LP) is 19.5% of the total normal force gradient for the automatic version in the tests, and 19.4% in the calculation (see Table 1). The good agreement between calculation and test, although the Mach numbers are different, validates the use of the ECOPAN code for the calculation of interaction effects.

Interpretation of Interaction Effects Due to Hermes

The difference between the normal force gradients on the lower part of the launcher for the automatic and Hermes versions ($\Delta C_{N\alpha}$LP, Table 1) is expressed in terms of the relative interaction of the flow from the Hermes wing by

$$(\Delta C_{N\alpha}\text{LP}/C_{N\alpha}\text{LP}_{\text{Auto}})$$

To characterize the increasing or decreasing stability due to the interaction, the position of the aerodynamic center of the interaction effect from Hermes on the lower part can be estimated by

$$Xf = Xm - (\Delta C_{M\alpha}\text{LP}/\Delta C_{N\alpha}\text{LP})L\text{ref}.$$

The values of the interactions as well as the corresponding center position evaluated from NLR tests and ECOPAN computations are given in Table 2.

A good agreement is noted between the computation and the tests concerning the interaction center position. These positions shown in Fig. 17 locate the interaction center 4.9 m forward of the c.g. of the launcher (computation and test averaging): this effect contributes to slowly limit the decreasing of stability effect due to the upper part itself (Hermes and adapter).

Table 2 Characterization of the interaction effect from Hermes to lower part

	Calculation $M = 0.5$	Test $M = 0.8$
$\Delta C_{N\alpha}$LP	−0.0245	−0.0380
$\frac{\Delta C_{N\alpha}\text{LP}}{C_{N\alpha}\text{LP}_{\text{Auto}}}$	−32%	−27%
Xf/Hermes nose	28.13 m	28.18 m

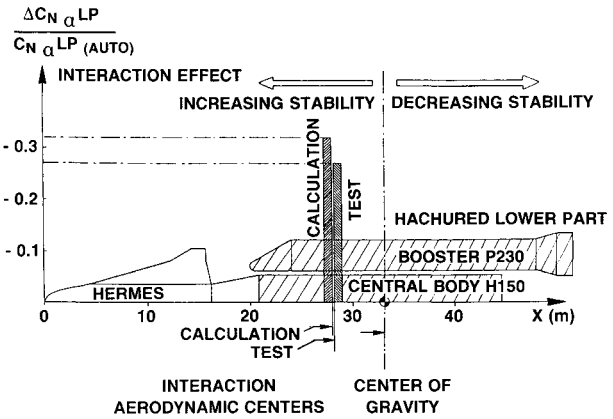

Fig. 17 Hermes interaction effect on lower part of launch vehicle.

Airbus Aircraft Applications

The first aircraft geometries studied were very simple with wing-fuselage-type configurations and simplificated wake geometries.

Preliminary Configuration Investigated: Wing-Fuselage Configuration with Prescribed Wake Sheet

A wing-fuselage configuration was quite appropriate for testing the method, particularly to verify the computation in the wake sheet-fuselage interaction zone. The mesh of the wing in the presence of an Airbus-type fuselage satisfies the constraint of regular closure at the trailing edge in order to assure a good junction with the wake sheet. The wing-fuselage grid set consists of 1537 panels. A prescribed wake lattice was defined next, with 510 panels; it starts along the trailing edge bisector of the wing along the line of the freestream velocity direction. Along the fuselage, the lattice is attached to a grid line corresponding approximately to a streamline, thereby making a relatively airtight junction.

A view of the whole grid is shown in Fig. 18, along with this wake lattice. This was used as input for the ECOPAN code. Figure 19 graphs an intermediate computation giving the doublet strength distribution over the surface, clearly showing the potential jump induced by the wake lattice along the fuselage.

The pressures are then calculated from the surface gradients of the potential, and more precisely of the doublet strengths, taking into account the absence of coupling between the domains located on either side of the discontinuity line on the fuselage. This potential jump induces no noticeable pressure discontinuity.

Later developments in the ECOPAN code have made it possible to consider much more complex and realistic geometries.

Computation of a Complete Aircraft in Takeoff Configurations

Computations of complete aircraft in takeoff configurations with flaps and slats extended requires industrially operational codes. The ECOPAN code was evaluated on an Airbus geometry in just such a configuration.

The grid consists of 10,250 panels, representing half the airplane. The wake sheets from the lifting surfaces (wing, leading-edge slat, flaps, and tail section) comprise 5800 doublet panels, with the various tip vortices being modeled by rolling up the wake sheets (Fig. 20). These lattices were generated on the basis of an initial flow streamline calculation, without any later calculation of a free-wake geometry. The landing gear is also taken into account, but an assumption of no-flow separation is carried out.

The engine primary and secondary fluxes are simulated by setting a normal velocity condition at the engine face section and an exhaust condition on the engine outlet section panels (Fig. 21). A pressure distribution calculated in the presence of wake lattices and engine jets is shown in Fig. 22.

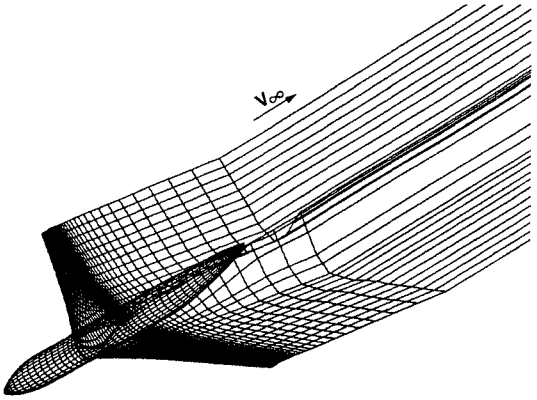

Fig. 18 Grid of a wing-fuselage configuration with wake lattice.

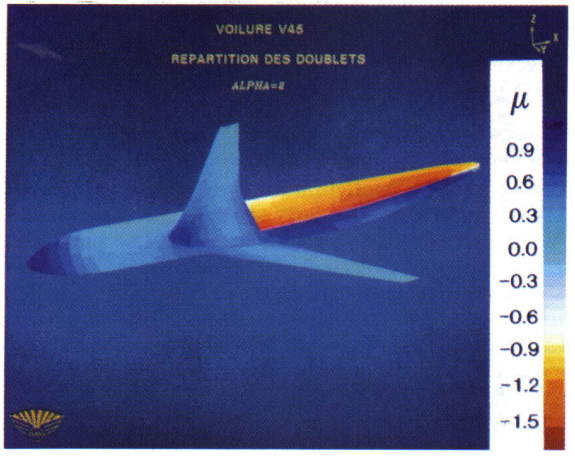

Fig. 19 Doublet strength field on the wing-fuselage configuration.

To simulate the ground effect on the aircraft, an implicit plane of symmetry is located at ground distance. The corresponding calculated pressure distribution is presented in Figs. 23 and 24. Both these pressure distributions show that the ECOPAN computation code has operated well on such a configuration: no particular numerical problems have been detected in the strong wake-fuselage interaction zones. The upper side view in Fig. 23 clearly shows a high suction at the leading edge, at the level of extended slats. This confirms that the high-lift devices, operating in this takeoff configuration, are well simulated. The wakes generated from the leading-edge slats are very close to the wing upper side and do not create any numerical problems.

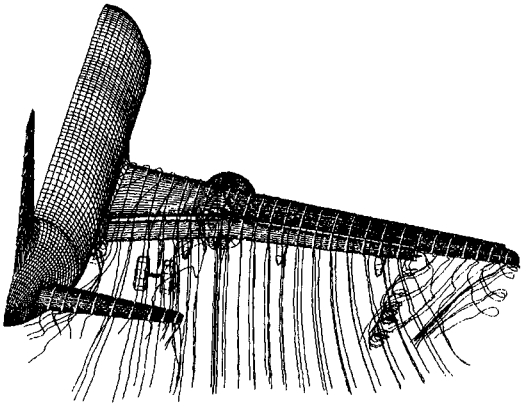

Fig. 20 Rear view of the Airbus grid (10,250 panels) from Aerospatiale.

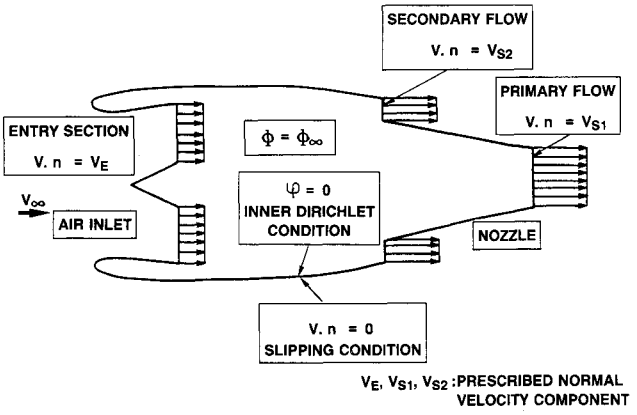

Fig. 21 Simulation of engine primary and secondary fluxes.

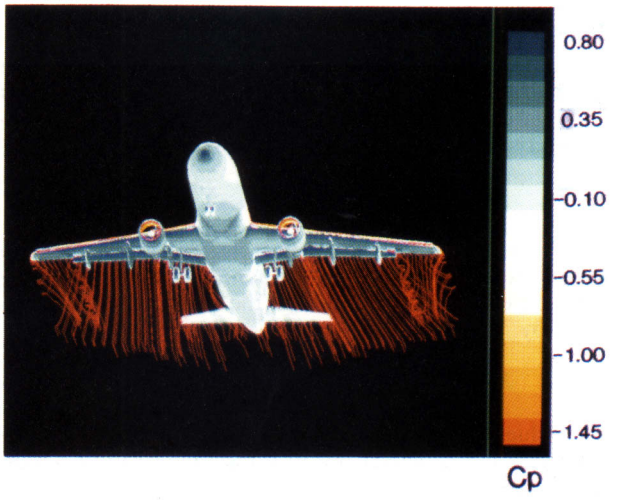

Fig. 22 Airbus front view with wake representation used for the computation.

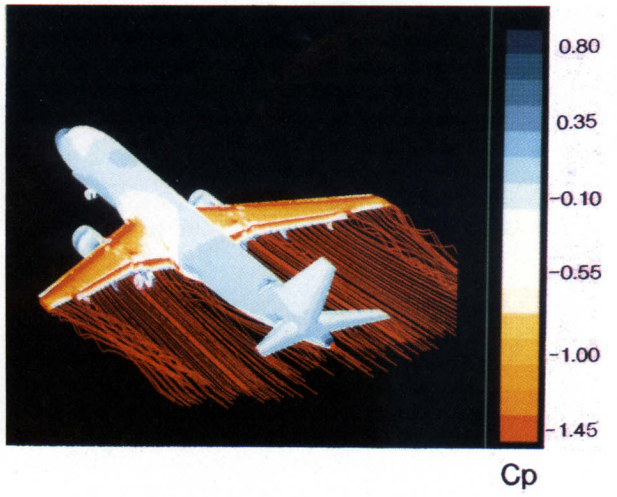

Fig. 23 Pressure field on Airbus type aircraft: ECOPAN calculation with ground effect.

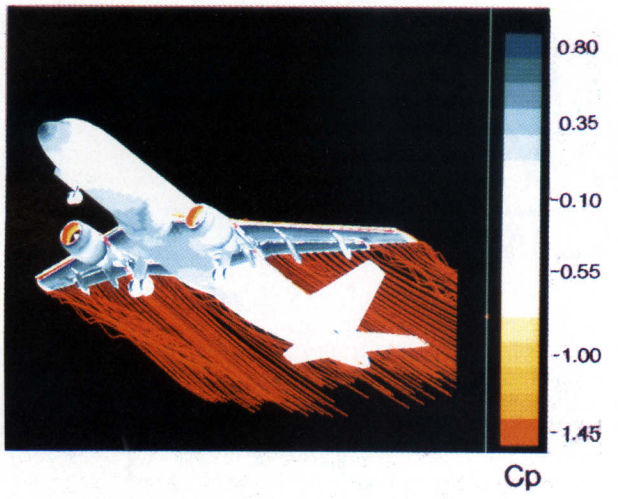

Fig. 24 Pressure field seen from underneath: ECOPAN calculation with ground effect.

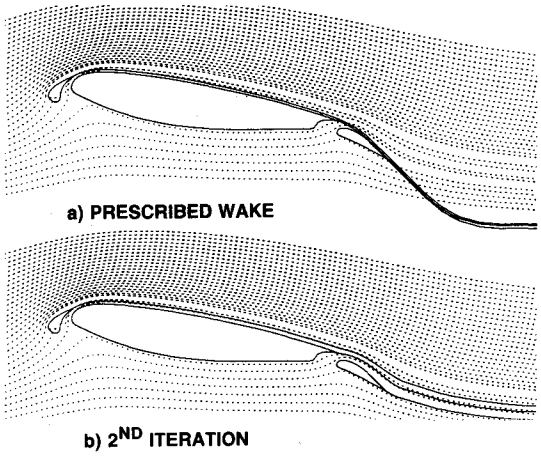

Fig. 25 Free-wake geometry calculation—two-dimensional configuration.

The pressure distributions were generated in a takeoff configuration with and without a plane of symmetry. By integrating both these pressure distributions, the ground effect can be estimated to be of the order of a few percents increase in lift for this computation case, which is in agreement with the flight test results. These results show that the ECOPAN code is operational. However, this preliminary calculation performed with a prescribed wake geometry does not prove that this code is able to presently determine the entire ground effect configurations. Nevertheless, some improvements could be made, such as a complete free-wake geometry calculation.

One encouraging free-wake geometry calculation has been performed in a two-dimensional configuration on a wing profile of this aircraft. Figure 25a presents the streamline calculation with a visualization of the estimated wake used as input for the calculation, and Fig. 25b shows the result after the second free-wake geometry iteration.

Conclusion

The ECOPAN code has demonstrated its versatility and operational status in a broad field of application. It is particularly well adapted to parametric analyses in subsonic flow.

A comparative analysis of the automatic and Hermes versions of the Ariane 5 launch vehicle has drawn out the most significant geometric effects on the longitudinal stability of the launcher. ECOPAN can determine differences in the longitudinal aerodynamic coefficient between the two Ariane 5 versions that are realistic, compared with the test results. The change from the automatic version to the Hermes version therefore results in overvelocities at the level of booster cones and in a decrease of the launcher total stability. This decrease is moderate by a favorable interaction of Hermes wake on the lower part of the launcher.

A comparative analysis of the forces applied to a complete Airbus geometry aircraft in takeoff configuration with flaps and slats extended and with the simulation of engine primary and secondary fluxes has been made. The increase in lift with a plane of symmetry simulating the ground effect has been estimated to be of the order of a few percents, which is in agreement with flight test results.

Acknowledgments

Ariane 5 applications have been carried out within the framework of Technical Assistance for the French space agency (CNES). Airbus aircraft applications were partly supported by the French Defense Ministry (STPA). The authors would like to thank Aerospatiale in providing the Airbus computational grids (airplane and wakes) and for the permission to publish the present results.

References

[1]Kirrmann, C., "Comparaison de Différentes Méthodes de Singularités pour le Calcul des Écoulements Internes en Tridimensionnel," TP ONERA 1984-150, Nov. 1984.

[2]Margason, R. J., Kjelgaard, S. O., Sellers, W. L., Morris, C. E. K., Walkley, K. B., and Shields, E. W., "Subsonic Panel Methods—A Comparison of Several Production Codes," AIAA Paper 85-0280, Jan. 1985.

[3]Strang, W. Z., Berdahl, C. H., Nutley, E. L., and Murn, A. J., "Evaluation of Four Panel Aerodynamic Prediction Methods (MCAERO, PAN AIR, QUADPAN and VSAERO)," AIAA Paper 85-4092, Oct. 1985.

[4]Clark, D. R., Maskew, B., and Dvorak, F. A., "The Application of a Second Generation Low-Order Panel Method—Program VSAERO—to Powerplant Installation Studies," AIAA Paper 84-0122, Jan. 1984.

[5]Ross, J. C., "Applicability of a Panel Method, Which Includes Nonlinear Effects, to a Forward-Swept-Wing Aircraft," AIAA Paper 84-2402, Oct. 1984.

[6]Smith, B. E., and Ross, J. C., "Application of a Panel Method to Wake Vortex/Wing Interaction and Comparison with Experiment," AIAA Paper 84-2182, Aug. 1984.

[7]Strash, D. J., Nathman, J. K., Maskew, B., and Dvorak, F. A., "The Application of a Low-Order Panel Method—Program VSAERO—to Powerplant and Airframe Flow Studies," AIAA Paper 84-2178, Aug. 1984.

[8]Liu, T. M., and Schaefer, R. W., "A Comparative Study of Computer Codes for Flow Field Calculation of Nacelle Inlets," AIAA Paper 86-0397, Jan. 1986.

[9]Miranda, L. R., "Application of Computational Aerodynamics to Airplane Design," AIAA Paper 82-0018, Jan. 1982.

[10]Baston, A., Lucchesini, M., Manfriani, L., Polito, L., and Lom-

bardi, G., "Evaluation of Pressure Distributions on an Aircraft by Two Different Panel Methods and Comparison with Experimental Measurements," International Council of the Aeronautical Sciences Paper 86-1.5.3, Sept. 1986.

[11]Fornasier, L., and Heiss, S., "Application of HISSS Panel Code to a Fighter-Type Aircraft Configuration at Subsonic and Supersonic Speeds," AIAA Paper 87-2619, Aug. 1987.

[12]Fornasier, L., and d'Espiney, P., "Prediction of Missile Stability Using the HISSS Panel Code," *Rech. Aérosp.*, No. 1989-4 (English and French editing), 1989, pp. 33–47.

[13]Snyder, L. D., and Erickson, L. L., "PAN-AIR Prediction of NASA Ames 12-Foot Pressure Wind Tunnel Interference on a Fighter Configuration," AIAA Paper 84-0219, Jan. 1984.

[14]Conner, R. S., and Purdon, D. J., "PAN-AIR Knowledge System," AIAA Paper 86-0239, Jan. 1986.

[15]Carr, M. P., "Accuracy Study of Transonic Flow Computation for 3D Wings," AGARD CP 437, May 1988.

[16]Le, T. H., Ryan, J., and Falempin, G., "Wake Modeling for Helicopter Fuselages," *Proceedings of the 13th European Rotorcraft Forum*, Associatory Aéronautique et Astronautique de France, Vol. 1, Paper 2–8, Arles, France, Sept. 1987; see also TP ONERA 1987–145, Sept. 1987.